High ionic conductivity in confined bismuth oxide-based heterostructures

Sanna, Simone; Esposito, Vincenzo; Christensen, Mogens; Pryds, Nini

Published in:
A P L Materials

Link to article, DOI:
10.1063/1.4971801

Publication date:
2016

Document Version
Publisher's PDF, also known as Version of record

High ionic conductivity in confined bismuth oxide-based heterostructures

Simone Sanna, Vincenzo Esposito, Mogens Christensen, and Nini Pryds

Citation: APL Mater. **4**, 121101 (2016); doi: 10.1063/1.4971801
View online: http://dx.doi.org/10.1063/1.4971801
View Table of Contents: http://aip.scitation.org/toc/apm/4/12
Published by the American Institute of Physics

High ionic conductivity in confined bismuth oxide-based heterostructures

Simone Sanna,[1] Vincenzo Esposito,[1] Mogens Christensen,[2] and Nini Pryds[1,a]
[1]*Department of Energy, Technical University of Denmark, DK-4000 Roskilde, Denmark*
[2]*Department of Chemistry and iNANO, Center for Materials Crystallography, Aarhus University, DK-8000 Aarhus C, Denmark*

(Received 26 September 2016; accepted 23 November 2016; published online 15 December 2016)

Bismuth trioxide in the cubic fluorite phase (δ-Bi_2O_3) exhibits the highest oxygen ionic conductivity. In this study, we were able to stabilize the pure δ-Bi_2O_3 at low temperature with no addition of stabilizer but only by engineering the interface, using highly coherent heterostructures made of alternative layers of δ-Bi_2O_3 and Yttria Stabilized Zirconia (YSZ), deposited by pulsed laser deposition. The resulting [δ-Bi_2O_3/YSZ] heterostructures are found to be stable over a wide temperature range (500-750 °C) and exhibits stable high ionic conductivity over a long time comparable to the value of the pure δ-Bi_2O_3, which is approximately two orders of magnitude higher than the conductivity of YSZ bulk.
[http://dx.doi.org/10.1063/1.4971801]

The charge and mass transport in oxide thin films could be tuned by the lattice strain engineering resulting in a new class of materials that can be considered fundamental bricks of new generation of devices for energy storage, conversion, and information.

Oxide heterostructures are a very promising type of artificial materials owing to possibility to manipulate the ionic and electronic properties at the interfaces by controlling the properties of the different layers, e.g., epitaxial strain.[1–6]

In these heterostructures, when the number of the interfaces is increased, size effects of the layers play a major role and can lead, for example, to enhanced mobility and conductivity of the charge carries at these interfaces.[2–6]

Due to their high ionic conductivity, thin films—bismuth-oxide-based materials—are good candidates for a number of applications, for example, multiferroics, ferroelectrics, gas sensors, light photocatalysts, solar cell, and fuel cells.[7–11] As a pure compound, bismuth oxide undergoes several phase transformations.[12] However, only the δ-Bi_2O_3 phase with face-centered cubic (fcc) structure exhibits high ionic conductivity in a narrow range of temperatures (730-825 °C).[12] The ionic conductivity of bismuth-oxide-based materials can reach ca. 1.8 S cm^{-1} at 750 °C.[12] Such values are due to the high concentration of oxygen vacancies in the δ-Bi_2O_3 phase structure, i.e., up to 25% of the oxygen site can be defective, and the high anion mobility in the crystal structure.[12–14]

Over the years, many attempts to stabilize the cubic phase to room temperature, e.g., by doping the bismuth with rare-earth oxides or transition metal oxides[13–16] or depositing thin film onto appropriate substrates by using different deposition techniques,[11,17–21] have been carried out.

More recently, we succeeded to stabilize the δ-Bi_2O_3 phase at room temperature by depositing alternating ultra-thin layers of bismuth-based oxide material stacked between fluorite materials.[11] This was done by creating alternating layers (~2.7 nm) of both $Ce_{0.8}Gd_{0.2}O_{2-\delta}$ (gadolinium-doped ceria; CGO) and $Er_{0.4}Bi_{1.6}O_3$ (erbium-stabilized bismuth; ESB) on MgO single crystals. As result,

[a]Author to whom correspondence should be addressed. Electronic mail: nipr@dtu.dk

the heterostructures remain stable without degradation under oxidizing and reducing conditions for a wide range of temperatures, and maintains high ionic conductivity characteristic of the typical bismuth oxide.

In this work, using a similar approach, we have fabricated thin films of pure bismuth oxide (without any acceptor solute dopants, such as Er^{3+}) confined within two layers of pure ionic conductor Yttria-Stabilized Zirconia (YSZ). The choice of using YSZ as a protective layer arises not only from its excellent chemical and thermal stability but also because it exhibits pure ionic conductivity without any electronic contribution at low oxygen partial pressure.[3,22–25]

Figure 1 shows a schematic illustration comparing the two heterostructures: 20 mol. % CGO and ESB deposited on a MgO (100) single crystal (Fig. 1(a)) and ZrO_2:8 mol. % Y_2O_3 (yttria stabilized zirconia) and Bi_2O_3 deposited on $NdGaO_3$ (100) single crystal (Fig. 1(b)), respectively. The multilayers in Figure 1 are defined as MgO/CGO/[ESB/CGO]$_N$ and NGO/YSZ/[Bi_2O_3/YSZ]$_N$ where N is the number of [ESB/CGO] and [Bi_2O_3/YSZ] bilayers, respectively. Figure 1 shows also an X-ray diffraction pattern taken in the out-of-plane direction of MgO/CGO/[ESB/CGO]$_{20}$ heterostructure (thickness ~60 nm) as well as NGO/YSZ/[Bi_2O_3/YSZ]$_{20}$ (thickness ~40 nm). For MgO/CGO/[ESB/CGO]$_{20}$ only the peak corresponding to (002) reflection is visible: satellite peaks are not resolved because CGO and ESB have very similar lattice parameters (5.44 Å and 5.46 Å, respectively) and the same fluorite structure; for more information see Ref. 11 (Fig. 1(c)). Conversely, for the [Bi_2O_3/YSZ] heterostructure in Fig. 1(d), having the lattice parameter of 5.26 Å at room temperature, the interference fringes are visible at the (111) orientation and the heterostructure shows high crystallographic quality also due to lower mismatch (3.8%) of the $NdGaO_3$ (100) substrate than on MgO (100). Indeed the

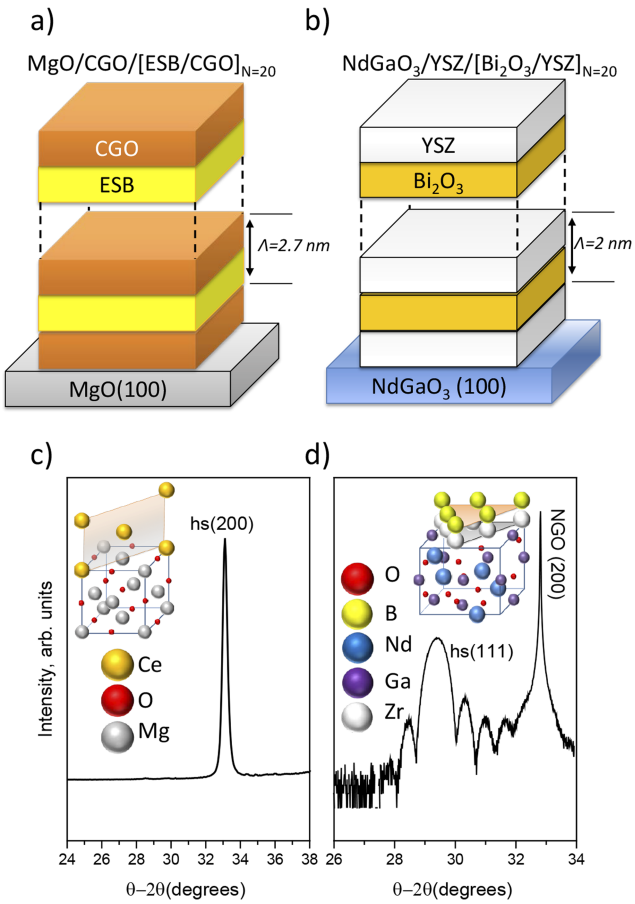

FIG. 1. Schematic illustration of heterostructures (hs) of MgO/CGO/[ESB/CGO]$_{N=20}$ with modulation length $\Lambda = 2.7$ nm (a) and heterostructures of NGO/YSZ/[Bi_2O_3/YSZ]$_{N=20}$ (b); the X-ray diffraction pattern of MgO/CGO/[ESB/CGO]$_{20}$ heterostructure with total thickness around 60 nm (c) and NGO/YSZ/[Bi_2O_3/YSZ]$_{20}$ with total thickness of 40 nm in logarithmic scale (d).

epitaxial relationship for the heterostructure CGO/[ESB/CGO]$_N$ (100) oriented onto the MgO (100) can be explained with a fluorite cubic cell of the film rotated 45° with respect to the MgO (100) substrate producing a misfit of ca. 9%. Conversely, the heterostructure based on [Bi_2O_3/YSZ] with (111) orientation can be described using a triangle lying on the perovskite orthorhombic structure of $NdGaO_3$ (100) producing an even lower misfit of ca. 3.8%.[3,17,26] A sketch of the relation between the substrate and the cubic fluorite is shown in Figures 1(c) and 1(d). Figure 2 shows the total conductivity measured at the in-plane direction versus 1000/T for the heterostructures NGO/YSZ/[Bi_2O_3/YSZ]$_{20}$, NGO/YSZ/Bi_2O_3/YSZ, and NGO/Bi_2O_3/YSZ with a thickness ratio of 1:1 and an overall thickness of about 40 nm. Electrical measurements were conducted by Electrochemical Impedance Spectroscopy (EIS) in the temperature range of 500-725 °C in air similar to our previous papers (see supplementary material).[11] The conductivity of Bi_2O_3 bulk and YSZ bulk is also given in Figure 2 for comparison.[12,22]

The total conductivity measured for these heterostructures increases slightly when the number of interfaces increases, reaching values of about two orders of magnitude larger than the conductivity of YSZ bulk[22] in the 500-725 °C temperature range (Fig. 2(a)). Particularly, the conductivity of the NGO/YSZ/[Bi_2O_3/YSZ]$_{20}$ as a function of the temperature exhibits two linear regions: from 475 to 600 °C where the activation energy is 1.49 eV, and then from 600 to 750 °C, where the activation energy has a value of 0.77 eV. The lower value of activation energy (see Figure 2(a)) corresponds to the activation energy of the pure of δ-Bi_2O_3 (dashed line).[11] This indicates that in the range of temperature 600-750 °C, the conductivity could be dominated by δ-Bi_2O_3. The changes in the activation energies could be due to order disorder transition that occurs at 600 °C.[12–16]

Figure 2(b) shows that the conductivity measurements, carried out over five days in the temperature range of 475-750 °C for the NGO/YSZ/[Bi_2O_3/YSZ]$_{20}$, exhibited the same trend already after three cycles, confirming the ability of the YSZ layers to preserve the structural and the electrical properties of the δ-Bi_2O_3 layers even below 730 °C, where the δ-Bi_2O_3 phase normally does not exist.[12]

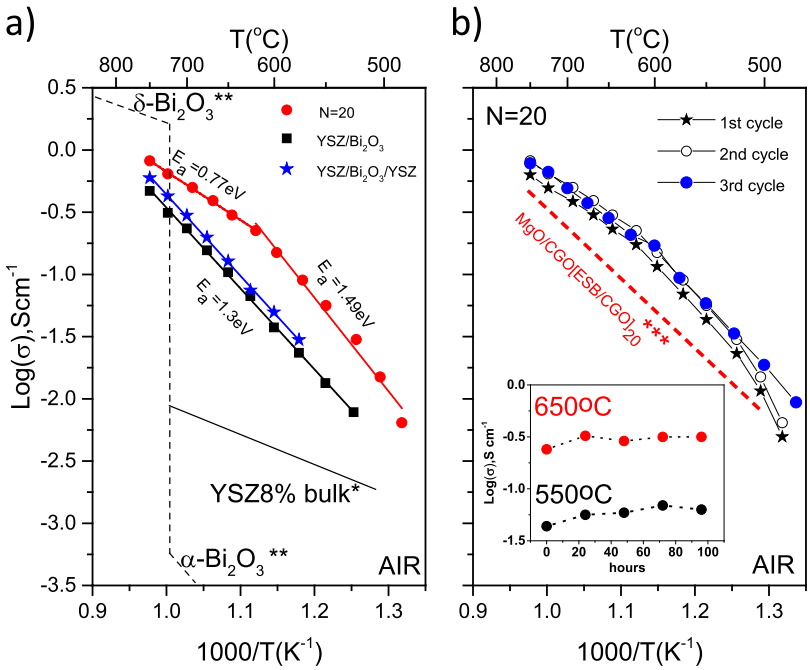

FIG. 2. Arrhenius plots of the in-plane conductivity for heterostructures NGO/YSZ/[Bi_2O_3/YSZ]$_{20}$, NGO/YSZ/Bi_2O_3/YSZ, and NGO/Bi_2O_3/YSZ with an Bi_2O_3/YSZ thickness ratio of 1:1 and an overall thickness of about 40 nm in the 475-750 °C temperature range in air atmosphere (a) and Arrhenius plots of the in-plane conductivity for heterostructures NGO/YSZ/[Bi_2O_3/YSZ]$_{20}$ after three cycles (b); in the inset in (b) the conductivity at 550 and 650 °C for over 100 h. The conductivity of YSZ bulk and δ-Bi_2O_3 bulk is reported for comparison (** = Ref. 12, * = Ref. 22). The dashed red line represents the Arrhenius plot of MgO/CGO/[ESB/CGO]$_{20}$ for comparison (*** = Ref. 11) (b).

The temperature was then set at 550 °C and 650 °C for 100 h in order to study the electrical stability as a function of time. In particular, as shown in the inset in Figure 2(b), the conductivity at 550 and 650 °C remains approximately constant for over 100 h, confirming the absence of ageing effects of the NGO/YSZ/$[Bi_2O_3/YSZ]_{20}$.

The reason for choosing different modulation length between [ESB/CGO] and $[Bi_2O_3/YSZ]$, for the film with N = 20, was due to the fact that the total conductivities were stable and reproducible for a long period of time only in the range of thickness, 2 and 2.7 nm, respectively. Therefore, we believe that there exists a critical thickness of the modulation length where the cubic fluorite structure CGO (gadolinium-doped ceria) and YSZ can confine and preserve the Bi_2O_3 in the cubic structure.

To confirm the phase stability of the δ-Bi_2O_3 confined in fluorite YSZ layers, NGO/YSZ/$[Bi_2O_3/YSZ]_N$ with N = 20 was investigated by HT-XRD (high temperature X-ray diffraction) in air and in N_2 atmosphere at a temperature range from room temperature to 750 °C (see Figure 3(a)). A sizeable increment of 15% of the lattice parameter in the out-of-plane direction from 5.26 Å to 5.40 Å can be observed when the temperature is increased from room temperature to 50 °C (Fig. 3(a)). On the other hand, in the temperature range between 50 °C and 750 °C, the lattice parameter *c* of the NGO/YSZ/$[Bi_2O_3/YSZ]_{20}$ was observed to only slightly increase and saturated at a value of 5.46 Å (see Fig. 3(a)). Albeit this jump of the value of lattice parameter *c* is evident, however, it is possible that the temperature of the sample in the range of 50-150 °C could be affected by the experimental error, i.e., the sensibility in the temperature of the thermocouple and the distance of it from the sample.

The change of the layers lattice parameter as function of the temperature is shown in Figure 3(b). At room temperature the lattice parameter is closer to the YSZ bulk sample (5.14 Å),[3] resulting in a compression strain of the δ-Bi_2O_3 (5.66 Å bulk[27,28]) phase while upon heating, the lattice parameter of the NGO/YSZ/$[Bi_2O_3/YSZ]_{20}$ increases resulting in relaxation of the δ-Bi_2O_3 layers through the interface with the YSZ layer.[29]

Remarkably, in this work we succeeded in stabilizing the pure δ-Bi_2O_3, by confining it in the YSZ cubic fluorite using a multilayered structure. The characterization results clearly demonstrate the fact that δ-phase of the pure Bi_2O_3 is able to persist also in the temperature ranges below 730 °C, where the δ-Bi_2O_3 phase normally does not exist. Furthermore, the ionic conductivity of the heterostructure remains stable for long period of time at values comparable to the typical values of pure δ-Bi_2O_3 phase. These findings open up a new frontier for designing new ionotronic materials and devices by stabilizing phases, using thin film confinement,[6] which otherwise are not thermodynamically stable.

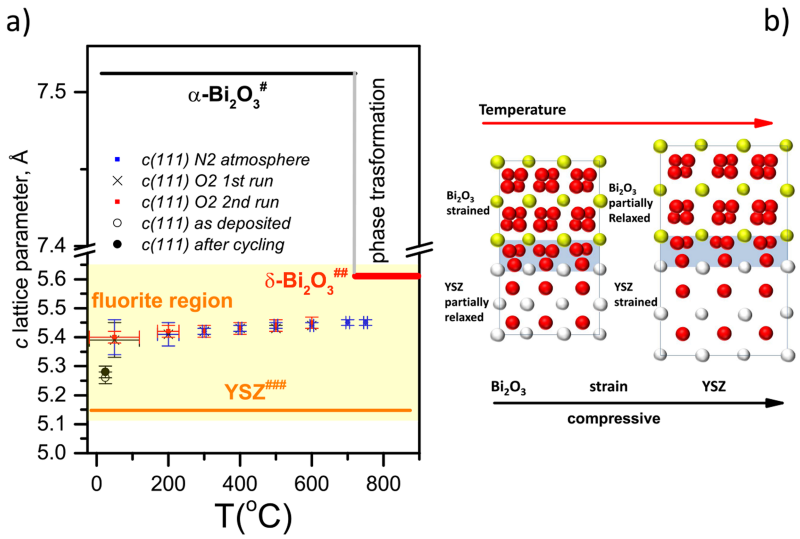

FIG. 3. Variation of lattice parameter out-of-plane of NGO/YSZ/$[Bi_2O_3/YSZ]_{20}$ heterostructure as a function of temperature and atmosphere (N_2, O_2). The lattice parameters of YSZ ($^{###}$ = Ref. 3), α-Bi_2O_3 ($^{#}$ = Ref. 27), and δ-Bi_2O_3 ($^{###}$ = Ref. 28) are reported for comparison (a); illustration of the strain of the fluorite cubic cell of Bi_2O_3 and YSZ as in function of the temperature (b).

NGO/YSZ/$[Bi_2O_3/YSZ]_{20}$, NGO/YSZ/Bi_2O_3/YSZ, and NGO/Bi_2O_3/YSZ, were grown by pulsed laser deposition (PLD) using a multi-target carousel. The PLD chamber was evacuated to a base vacuum of 1×10^{-7} mbar before the deposition took place. A KrF excimer laser (Coherent Lambda Physik GmbH) with a wavelength of 248 nm and pulse duration of 25 ns was focused on the target. The laser energy density was kept constant at 2 J cm^{-2} with a repetition rate of 2 Hz. The temperature and the oxygen partial pressure of the substrate during the deposition were 600 °C and 10^{-2} mbar, respectively. The distance target substrate was kept constant at 50 mm. The modulation length was tuned by varying the number of laser shots on the targets. The deposition rate for Bi_2O_3 and YSZ was calibrated to be about 0.05 Å per pulse.

XRD characterization. θ-2θ scans and rocking curve analysis were performed using the Rigaku Smartlab diffractometer. The X-ray beam is monochromatized and focused by a one-dimensional multilayer optic (λ = 1.5418 Å) with a rotating Cu anode as a source, operating at 40 kV and 200 mA.

Electrical characterization. Electrochemical impedance spectroscopy (EIS) measurements were carried out in a two-electrode configuration geometry using silver paste electrodes painted on the film surface. EIS measurements were performed in the 475-750 °C temperature range and 50 Hz-1 MHz frequency range, with a 0.2 V alternating voltage signal (see supplementary material). EIS measurements were performed in air.

See supplementary material for electrical characterization.

[1] M. Moors, K. K. Adepalli, Q. Lu, A. Wedig, C. Bäumer, K. Skaja, B. Arndt, H. L. Tuller, R. Dittmann, R. Waser, B. Yildiz, and I. Valov, ACS Nano **10**, 1481 (2016).
[2] S. Schweiger, M. Kubicek, F. Messerschmitt, C. Murer, and J. L. M. Rupp, ACS Nano **8**(5), 5032 (2014).
[3] S. Sanna, V. Esposito, A. Tebano, S. Licoccia, E. Traversa, and G. Balestrino, Small **6**, 1863 (2010).
[4] A. Fluri, D. Pergolesi, V. Roddatis, A. Wokaun, and T. Lippert, Nat. Commun. **7**, 1 (2016).
[5] N. Sata, K. Eberman, K. Eberl, and J. Maier, Nature **408**, 946 (2000).
[6] N. Pryds and V. Esposito, "When two become one: An insight into 2D conductive oxide interfaces," J. Electroceram. (published online, 2016).
[7] B. H. Park, B. S. Kang, S. D. Bu, T. W. Noh, J. Lee, and W. Jo, Nature **401**, 682 (1999).
[8] J. Wang, J. B. Neaton, H. Zheng, V. Nagarajan, S. B. Ogale, B. Liu, D. Viehland, V. Vaithyanathan, D. G. Schlom, U. V. Waghmare, N. A. Spaldin, K. M. Rabe, M. Wuttig, and R. Ramesh, Science **299**, 1719 (2003).
[9] W. M. Sears, Sens. Actuators **19**, 351 (1989).
[10] K. Gurunathan, Int. J. Hydrogen Energy **29**, 933 (2004).
[11] S. Sanna, V. Esposito, J. W. Andreasen, J. Hjelm, W. Zhang, T. Kasama, S. B. Simonsen, M. Christensen, S. Linderoth, and N. Pryds, Nat. Mater. **14**, 500 (2015).
[12] P. Shuk, H. D. Wiemhoefer, U. Guth, W. Göpel, and M. Greenblatt, Solid State Ionics **89**, 179 (1996).
[13] N. Jiang and E. D. Wachsman, J. Am. Ceram. Soc. **82**, 3057 (1999).
[14] S. Boyapati, E. D. Wachsman, and B. C. Chakoumakos, Solid State Ionics **138**, 293 (2001).
[15] S. Boyapati, E. D. Wachsman, and N. Jiang, Solid State Ionics **140**, 149 (2001).
[16] E. D. Wachsman, G. R. Ball, N. Jiang, and D. A. Stevenson, Solid State Ionics **52**, 213 (1992).
[17] S. Sanna, V. Esposito, C. Graves, J. Hjelm, J. W. Andreasen, and N. Pryds, Solid State Ionics **266**, 13 (2014).
[18] C. L. Gomez, O. Depablos-Rivera, J. C. Medina, P. Silva-Bermudez, S. Muhl, A. Zeinert, and S. E. Rodil, Solid State Ionics **255**, 147 (2014).
[19] P. L. Popa, S. Sønderby, S. Kerdsongpanya, J. Lu, N. Bonanos, and P. Eklund, J. Appl. Phys. **113**, 046101 (2013).
[20] J. A. Switzer, M. G. Shumsky, and E. W. Bohannan, Science **284**, 293 (1999).
[21] G. Szwachta, S. Kąc, and T. Moskalewicz, Surf. Coat. Technol. **302**(25), 474 (2016).
[22] V. V. Kharton, F. M. B. Marques, and A. Atkinson, Solid State Ionics **174**, 135 (2004).
[23] J.H. Joo and G. M. Choi, Solid State Ionics **177**, 1053 (2006).
[24] I. Kosacki, T. Suzuki, V. Petrovsky, and H. U. Anderson, Solid State Ionics **136-137**, 1225 (2000).
[25] I. Kosacki, C. M. Rouleau, P. F. Becher, J. Bentley, and D. H. Lowndes, Solid State Ionics **176**, 1319 (2005).
[26] S. Sanna, V. Esposito, D. Pergolesi, A. Orsini, A. Tebano, S. Licoccia, G. Balestrino, and E. Traversa, Adv. Funct. Mater. **19**, 1713 (2009).
[27] S. A. Ivanov, R. Tellgren, H. Rundlof, and V. G. Orlov, Powder Diffr. **16**(4), 227 (2001).
[28] S. Hull, S. T. Norberg, M. G. Tucker, S. G. Eriksson, C. E. Mohn, and S. Stolen, Dalton Trans. **2009**(40), 8737.
[29] K. M. Kant, V. Esposito, and N. Pryds, Appl. Phys. Lett. **100**, 033105 (2012).